4

Ultrafine and Fine Aerosol Deposition in the Nasal Airways of a 9-Month-Old Girl, a 5-Year-Old Boy and a 53-Year-Old Male

Jinxiang Xi[1,2], JongWon Kim[1] and Xiuhua A. Si[3]
[1]*University of Arkansas at Little Rock, Little Rock, AR,*
[2]*Central Michigan University, Mount Pleasant, MI*
[3]*Calvin College, Grand Rapids, MI,*
USA

1. Introduction

Exposure to environmental aerosols of submicrometer size may cause significant risks to human health. Submicrometer aerosols include particles in the ultrafine (<100 nm) and fine (100 nm to 1 μm) regimes. Recent studies indicate that aerosols in this size range are biologically more active and potentially more toxic than micrometer particles of the same material (Kreyling et al., 2006; Kreyling et al., 2004; Li et al., 2003; Oberdorster and Utell 2002). Sources of submicrometer aerosols include diesel exhaust (50 to 500 nm) (Kittelson 1998), cigarette smoke (140 to 500 nm) (Bernstein 2004; Keith 1982), and radioactive decay (1 to 200 nm) (ICRP 1994). Submicrometer bioaerosols include respiratory specific viruses such as Avian flu and SARS, which typically range from 20 to 200 nm (Mandell et al., 2004). These aerosols may deposit in the respiratory airways in discrete amounts resulting in local injury and spread of infectious diseases. Considering the extrathoracic nasal airways, which include the nasal passages, pharynx, and larynx, the deposition of submicrometer aerosols is associated with a number of detrimental health effects. The deposition of cigarette smoke particles has been quantitatively linked to the formation of respiratory tract tumors at specific sites (Martonen 1986). Yang et al. (1989) reported that respiratory tract cancers per unit surface area are approximately 3,000 times more likely in the extrathoracic airways including the larynx. Ostiguy et al. (2008) summarized the adverse health effects due to various nanoparticles such as carbon nanotubes, fullerenes, inorganic and organic nanoparticles, and quantum dots. Gurr *et al*. (2005) studied the effect of ultrafine TiO2 particles on human bronchial epithelial cells and reported that TiO2 particles of 10 and 20 nm triggered oxidative DNA damage and lipid peroxidation, the later of which may also explains the cytotoxicity of water-soluble fullerenes or nC60 (Sayes *et al*., 2005).

Compared to adults, infants and children are more susceptible to respiratory risks. Exposure to ambient toxicants in children may cause adverse effects such as nasal obstruction, sinusitis, nasal carcinomas, and spread of infectious diseases. Respiratory disease remains a leading cause of childhood morbidity in the U.S. and other developed countries and is a leading cause to childhood deaths worldwide (U.S. Surgeon General Report 2007). Epidemiological studies have shown that children are biologically more susceptible to

particulate matters (PM) than adults due to their immature defense mechanism and detoxification pathways (U.S. Surgeon General Report 2007). Besides, children usually spend more time outdoors, breath faster, and therefore may receive a greater dose of PM than adults. Those children with a history of asthma often exhibit elevated levels of other respiratory symptoms such as cough, bronchitis, or pneumonia when living in highly polluted areas (California EPA 2005). Passive tobacco smoke exposure can also cause different health problems. Specifically, it (1) increases the frequency and severity of children's cold, sore throat, and asthma, (2) aggravates sinusitis, rhinitis, cystic fibrosis, and chronic respiratory problems, and (3) causes recurrent ear infections (California EPA 2005).

In contrast with potentially negative health effects, inhalation therapy for infants and children has been employed to deliver pharmaceutical aerosols to the lung via nasal route or to the nasal passages as the direct target. Aerosol delivery issues specific to children include lower tidal volumes, smaller airway size, and use of mask versus mouthpiece. Only a small amount of the applied dose reaches the target receptor in children. Studies have shown that for adults about 10% of the administered drug reaches the lung whereas for infants and toddlers this percentage is usually less than 1% (Everard 2003). Therefore, children adapted methods, dose, and devices are likely to increase therapeutic options leading to improved inhalation therapy and medical outcomes.

A number of *in vivo* and *in vitro* studies have considered the deposition of submicrometer aerosols in the nasal airway. *In vitro* studies that evaluated the nasal deposition of ultrafine aerosols in humans include Cheng et al. (1996a) and Swift and Strong (1996). The study of Cheng et al. (1996a) considered the deposition of aerosols ranging from 4 – 150 nm in 10 subjects and quantified variability in nasal geometries using MRI scans. Deposition was shown to be a function of nasal cavity surface area, minimum cross-sectional area, and shape complexity. *In vitro* studies provide the advantage of avoiding human subject testing and can determine depositions within specific regions of the nasal cavity. A number of *in vitro* studies have considered deposition of ultrafine aerosols in replicas of human noses (Cheng 2003; Cheng et al., 1993; Cheng et al., 1988; Gradon and Yu 1989; Guilmette et al., 1994; Kelly et al., 2004b; Yamada et al., 1988). The nasal geometries used in these studies are typically derived from medical scan data (CT and MRI) or casts of cadavers. Results of the available *in vitro* experiments are in general agreement with the deposition data from *in vivo* studies for ultrafine aerosols (Cheng et al., 1996a). Based on a collection of *in vivo* nasal deposition studies, Cheng et al. (1996b) suggested a best-fit correlation for particle sizes less than 150 nm. Later, Cheng et al. (2003) incorporated *in vivo* and *in vitro* nasal deposition data of ultrafine and micrometer particles to develop a correlation for particle sizes in the diffusional and the impaction deposition regimes. A common disadvantage of both *in vivo* and *in vitro* methods is the difficulty in determining local deposition values.

Previous numerical studies have considered the transport and deposition of fine and ultrafine particles in the nasal cavity (Liu et al., 2007; Martonen et al., 2003; Schroeter et al., 2001; Shi et al., 2006; Xi and Longest 2008; Xi and Longest 2009; Yu et al., 1998; Zamankhan et al., 2006). Similar CFD studies have also evaluated the transport and absorption of dilute chemical species in the nasal passages (Cohen Hubal et al., 1996; Scherer et al., 1994; Zhao et al., 2004). Compared with *in vitro* and *in vivo* studies, CFD predictions have the advantage of providing detailed information on airflow and aerosol deposition, like hot spots that are more relevant to health outcome than the average deposition. However, to the authors' knowledge, very few CFD studies have been reported so far studying children nasal

depositions, with one exception being Xi et al. (2011) that examined the transport and depositions of micrometer particles. The general neglect of child or infant nasal airways in previous studies may largely attribute to limited accessibility of pediatric medical images to CFD practitioners as well as the complexities involved in constructing physiologically realistic nasal passages. Concerning the age-related effect, several investigators have evaluated lung depositions of micrometer aerosols using scaled-down tracheobronchial models representative of growing lungs at different ages (Asgharian et al., 2004; Crawford 1982; Oldham et al., 1997; Xu and Yu 1986). In these studies, significant variations in micrometer particle lung deposition with respect to age were observed, with higher deposition in children than adults. However, no numerical study has considered the age-related effects upon the nasal deposition of ultrafine and fine-regime aerosols.

The objective of this chapter is to assess the age effects on airflow and aerosol dynamics within the nasal cavity in a systemic manner. There are three specific goals in this study: (1) quantifying morphologic dimensions of the nasal airway models for a 9-month-old girl, a 5-year-old boy, and a 53-year-old adult; (2) numerically characterizing the breathing resistance, airflow dynamics, and particle transport within the nasal passages during inhalation; and (3) numerically evaluating the deposition of submicrometer aerosols in the infant, child, and adult nasal airways on a total, sub-regional, and localized basis. Results of this study may lead to a better understanding of the developmental respiratory physiology and the associated effects on children's health response to environmental pollutants, or the medical outcome from inhalation therapy for infants and children.

Parameter	Range
d_p (nm)	Ultrafine: 1, 2, 3, 5, 10, 20, 50, 100 Fine: 100, 200, 300, 400, 500, 700, 1,000
Flow rate Q_{in} (L/min)	3, 5, 7.5, 10, 15, 20, 30, 45
Cunningham correction factor C_c	221 – 1.15
Particle diffusivity $\tilde{D}$ (cm²/s)	5.44×10^{-2} – 2.84×10^{-7}
Schmidt number $Sc = \nu / \tilde{D}$	2.92 – 5.61×10^{-5}
Particle Stokes number St_k	2.4×10^{-8} – 3.0×10^{-3}
Flow Reynolds number at the inlet	189 – 5,243

Table 1. Test conditions for the three airway models

2. Methods

To achieve the above goals, anatomically realistic nasal airway models have been constructed based on CT/MRI images. Breathing scenarios ranging from sedentary through heavy activity conditions (i.e., 3–30 L/min) and inhaled particles ranging from 1 nm to 1,000 nm are considered (Table 1). Details of the geometry construction, inhalation conditions, and particle transport models are described below.

2.1 Construction of the nasal airway models

For inhalation toxicology and pharmaceutical research, imaged-based modeling represents a significant improvement compared with conventional cadaver casting, which is subject to

distortion due to the shrinkage of mucous membranes or insertion of casting materials. Pritchard and McRobbie (2004) compared a cadaver cast with their MRI oropharyngeal airway model averaged over 20 subjects (10 males and 10 females) and showed significant geometric disparities. The most prominent difference was the greater volume of the cadaver casts, which was 92.7 cm^3 for the cast versus 46.7 cm^3 (SD12.7) for imaging. Generally, a physical model produced from anatomical images results in about 5% difference in the airway volume and some loss of fine morphological details. Therefore, this approach may adequately approximate the internal geometries (Pritchard and McRobbie 2004).

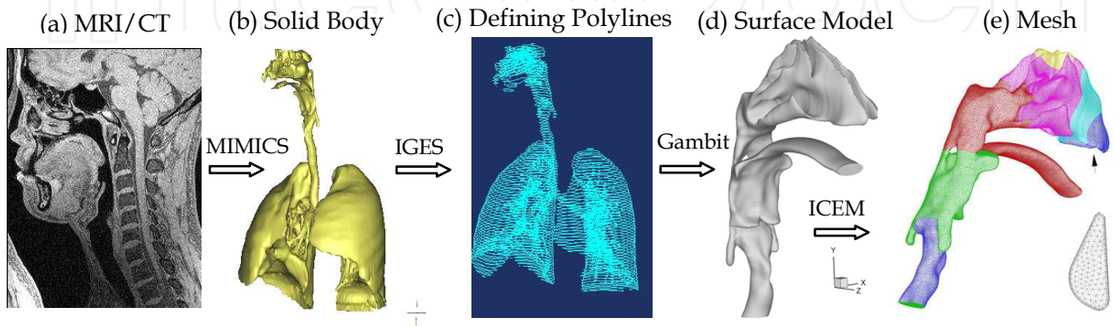

Fig. 1. Procedures of 3D rendering of CT/MRI images.

We will use one example to illustrate the computer method for developing a surface model of the respiratory tract based on medical images such as CT or MRI data. Figures 1a–e illustrate the procedure of translating from CT scans into a high-quality computational mesh of the nasal-laryngeal airway (Xi et al. 2010). To construct the 3D airway model, CT scans of a healthy non-smoking 53-year-old male (weight 73 kg and height 173 cm) were used, which were obtained with a multirow-detector helical CT scanner (GE medical systems, Discovery LS) and the following acquisition parameters: 0.7 mm effective slice spacing, 0.65 mm overlap, 1.2 mm pitch, and 512×512 pixel resolution. The multi-slice CT images were then imported into MIMICS (Materialise, Ann Arbor MI) and were segmented according to the contrast between osseous structures and intra-airway air to convert the raw image data into a set of cross-sectional contours that define the solid geometry (Figs. 1a–c). Based on these contours, a surface geometry was constructed in Gambit 2.3 (Ansys, Inc.) (Fig. 1d). The surface geometry was then imported into ANSYS ICEM (Ansys, Inc.) as an IGES file for meshing. Due to the high complexity of the model geometry, an unstructured tetrahedral mesh was created with high-resolution pentahedral elements in the near-wall region (Fig. 1e). The main geometric features retained in this example include nasal passages, nasopharynx (NP), pharynx, and throat. In particular, anatomical details such as uvula, epiglottal fold, and laryngeal sinus are retained. The resulting model is intended to faithfully represent the anatomy of the extrathoracic airway with only minor surface smoothing. Similarly, MRI scans of a healthy 5-year-old boy (weight 21 kg and height 109 cm) and CT scans of a 9-month-old girl (weight and height unknown) were used in this study to construct the pediatric nasal airway models. In order to quantitatively evaluate the flow field and aerosol depositions within the nasal airway, the airway model is divided into different sections (Fig. 2). In the main flow direction, subregions include the nasal vestibule and valve region (V&V), turbinate region (TR), nasopharynx (NP), pharynx and larynx. On top of the nasal airway is the olfactory region (OR) where the sensory nerves are located.

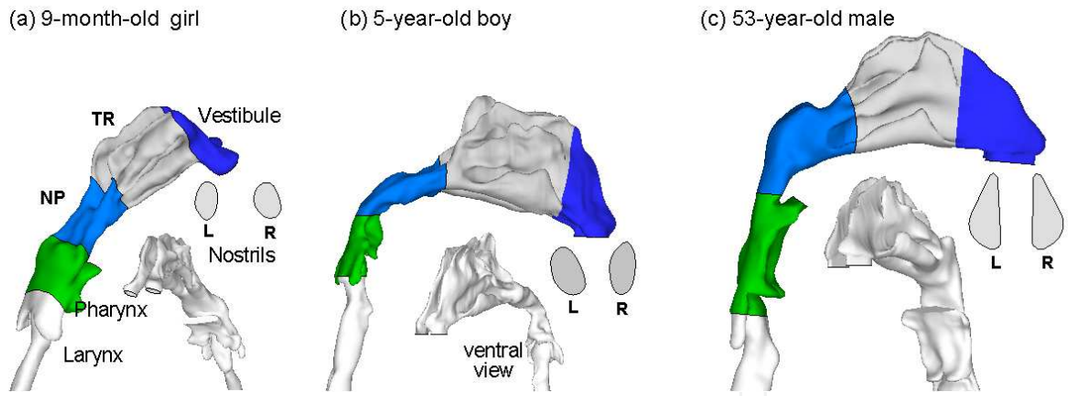

Fig. 2. Image-based nasal-laryngeal airway models.

2.2 Boundary conditions

Steady inhalation was assumed for all simulations with uniform velocity profiles at both nose inlets (nostrils) (Fig. 2). Initial particle velocities were assumed to be the same as the local fluid velocity. The airway surface was assumed to be smooth and rigid with no-slip (u_{wall} = 0) and perfect absorption conditions. In the body, the extrathoracic airway is covered with a thin layer of mucus, which captures particles at initial contact and clears them to the throat or nasal vestibule by mucocilliary movement within a time period of 10 to 15 minutes. Mass diffusion and metabolism of deposited particles may occur within the mucus layer and may change the zero-concentration conditions at the wall. However, due to the slow speed of the mucocilliary movement compared with the intranasal airflow and relatively low deposition rates, the no-slip and perfect absorption conditions are reasonable approximations in this study.

2.3 Fluid and particle dynamics equations

Flows in this study are assumed to be isothermal and incompressible. The mean inlet Reynolds number at the trachea varies from 368 to 3,302. The maximum Reynolds number based on the hydraulic diameter of the glottal aperture is approximately 8,037. Multi-regime flow dynamics can coexist in the nasal airway due to its unique physiology. To resolve the possible laminar-transitional-turbulent flow conditions, the low Reynolds number (LRN) k-ω model was selected based on its ability to accurately predict pressure drop, velocity profiles, and shear stress for transitional and turbulent flows. Moreover, the LRN k-ω model was shown to provide an accurate solution for laminar flow as the turbulent viscosity approaches zero (Wilcox 1998).

The transport and deposition of the submicrometer particles are simulated with a well-tested discrete Lagrangian tracking model enhanced with near-wall treatment. The aerosols evaluated in this study had a density of 1.0 g/cm^3 and particle Stokes number ($St_k = \rho_p d_p^2 U/18\mu D_h$) range of 0.00001 to 1.0. The inhaled particles were assumed to be dilute and had no influence upon the continuous-phase, i.e., one-way coupled particle motion. In our previous studies, the Lagrangian tracking model enhanced with user-defined routines was shown to provide close agreement with experimental deposition data in upper respiratory airways for both submicrometer (Xi et al., 2008) and micrometer particles (Xi and Longest 2007). The discrete Lagrangian transport equations can be expressed as

$$\frac{dv_i}{dt} = \alpha \frac{Du_i}{Dt} + \frac{f}{\tau_p}(u_i - v_i) + g_i(1-\alpha) + f_{i,Brownian} \text{ and } \frac{dx_i}{dt} = v_i(t) \quad (1)$$

where v_i and u_i are the components of the particle and local fluid velocity, and τ_p (i.e., $\rho_p d_p^2/18\mu$) is the characteristic time required for a particle to respond to changes in the flow field. The drag factor f, which represents the ratio of the drag coefficient C_D to Stokes drag, is based on the expression of Morsi and Alexander (1972). The influence of non-uniform fluctuations in the near-wall region is taken into account by implementing an anisotropic turbulence model proposed by Matida et al. (2004), which is described as

$$u'_n = f_v \xi \sqrt{2k/3} \quad and \quad f_v = 1 - \exp(-0.002y^+) \quad (2)$$

In this equation, ξ is a random number generated from a Gaussian probability density function and f_v is a damping function component normal to the wall for values of y^+ less than 40. Away from the wall ($y^+ > 40$), $f_v = 1$.

Evaluation of the particle trajectory equation requires that the fluid velocity u_i be determined at the particle location for each time-step. On a computational grid, determining the fluid velocity at the particle location requires spatial interpolation from control-volume centers or nodal values. Based on studies of deposition in the oral airway using Fluent 6, fluid velocities in wall-adjacent control volumes were observed to maintain the value at the control-volume center and not approach zero at the wall (Longest and Xi 2007). Longest and Xi (2007) reported that a near-wall interpolation (NWI) algorithm provided an effective approach to accurately predict the deposition of nanoparticles in the respiratory tract. A user-defined routine was developed that linearly interpolates the fluid velocity in near-wall control-volumes from nodal values. Velocity values at the wall were taken to be zero.

2.4 Numerical method and convergence sensitivity analysis

To solve the governing mass and momentum conservation equations in each of the cases considered, the CFD package ANSYS Fluent 6.3 was employed. User-supplied Fortran and C programs were implemented for the calculations of inlet flow and particle profiles, particle transport and deposition locations, grid convergence, and deposition enhancement factors. A specific set of user-defined functions was also applied for implementing the anisotropic turbulence effect and near-wall velocity interpolation. All transport equations were discretized to be at least second order accurate in space. A segregated implicit solver was employed to evaluate the resulting linear system of equations. This solver uses the Gauss-Seidel method in conjunction with an algebraic multigrid approach for improving the calculation performance on tetrahedral meshes. Convergence of the flow field solution was assumed when the global mass residual was reduced from its original value by five orders of magnitude and when the residual-reduction-rates for both mass and momentum were sufficiently small.

The computational meshes of the four nasal-laryngeal airway models were generated with ANSYS ICEM 12.0 (Ansys, Inc.). An unstructured tetrahedral mesh was generated with high-resolution prismatic cells in the near-wall region (Fig. 3) to accommodate the high complexity of the model geometry. A grid sensitivity analysis was conducted by testing the effects of different mesh densities with approximately 540,200, 980,900, 1,750,000 and

2,812,000 control volumes while keeping the near-wall cell height constant at 0.05 mm (Xi et al., 2008). Increasing grid resolution from 1,750,000 to 2,812,000 control volumes resulted in total deposition changes of less than 1%. As a result, the final grid for reporting flow field and deposition conditions consisted of approximately 1,750,000 cells with a thin five-layer pentahedral grid in the near-wall region and a first near-wall cell height of 0.05 mm.

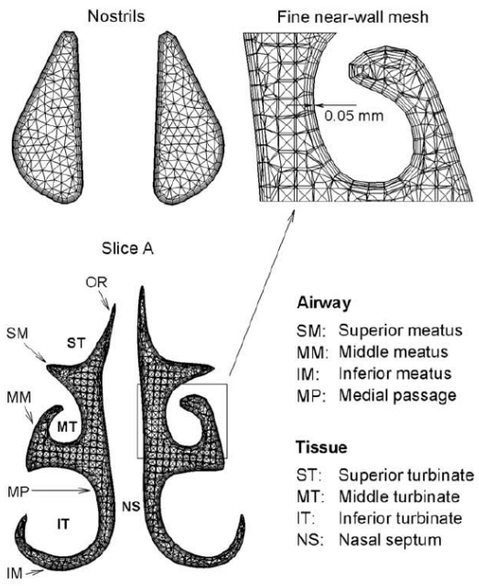

Fig. 3. Coronal view of the ICEM-generated computational mesh of the 53-year-old male.

For discrete Lagrangian tracking, the number of seeded particles required to produce count-independent depositions was tested. Particle count sensitivity analysis was performed by incrementally releasing groups of 10,000 particles. The number of groups was increased until the deposition rate changed by < 1%. The final number of particles tracked for ultrafine and fine-regime aerosols were 60,000 and 100,000 respectively.

3. Results

3.1 Infant-child-adult discrepancy

The differences of nasal airways among a 9-month-old girl, a 5-year-old boy (Xi et al., 2011) and a 53-year-old male reported previously (Xi and Longest 2008) are quite obvious in both morphology and dimensions. As for the morphology, younger subjects have smaller sized nostrils, shorter turbinate regions, longer but thinner nasopharynx, and thinner pharynx-larynx. It is therefore expected that as a human grows from birth to adulthood, the airway geometry keeps changing, which in turn alters the nasal aerodynamics as well as the deposition patterns of inhaled aerosols.

A quantitative comparison of airway dimensions among these three subjects is shown in Fig. 4 in terms of coronal cross-sectional area and hydraulic diameter d_h, both as a function of distance from the nose tip. Comparison of airway volume and surface area among the three subjects for various nasal anatomical sections are listed in Table 2. The dimension of two nostrils and upper trachea are shown in Table 3. It is noted that the test conditions (such as geographical elevation) are not clear for these three subjects, and the differences

Anatomical sections*	Volume, V (cm^3)			Surface area, A (cm^2)			Effective diameter, d_e‡ (cm)		
	9-m	5-yr	Adult	9-m	5-yr	Adult	9-m	5-yr	Adult
V&V	1.25	3.37	5.50	9.75	23.74	35.58	0.512	0.568	0.619
TR	2.83	11.03	12.63	35.63	107.34	112.59	0.318	0.411	0.449
NP	1.74	3.95	16.33	9.27	15.27	40.93	0.750	1.034	1.595
Pharynx	3.19	2.64	13.89	13.71	14.59	45.10	0.932	0.724	1.232
Larynx	1.32	1.22	6.70	8.37	7.20	21.81	0.629	0.676	1.228
Total	10.33	22.21	55.05	76.73	168.14	256.01	0.538	0.528	0.860

* V&V (vestibule and valve region), TR (turbinate region), NP (nasopharynx)
‡ Effective diameter $d_e = 4V/A$

Table 2. Comparison of nasal airway dimension among an infant, a child and an adult.

Anatomical sections	Cross-sect area, A (mm^2)			Perimeter, P (mm)			Hydr. diameter, d_h‡ (mm)		
	9-m	5-yr	Adult	9-m	5-yr	Adult	9-m	5-yr	Adult
R nostril	27.98	49.20	101.27	19.92	25.61	44.53	5.62	7.68	9.10
L nostril	31.48	43.74	101.27	20.49	24.89	44.53	6.15	7.03	9.10
Trachea	50.64	83.23	148.66	25.59	33.59	45.66	8.01	9.91	13.02

‡ Hydraulic diameter $d_h = 4A/P$

Table 3. Dimension of the nostrils and upper trachea of the three airway models.

presented herein are assumed to be mainly attributed to the age effect. From Table 2, the nasal airway volume of the 9-month-old infant and the 5-year-old child is 18.8% and 40.3% that of the adult, respectively; while the nasal airway surface area of the infant and child is 30.0% and 65.7% that of the adult, respectively. In particular, two major disparities are noted. First, the infant and child both possess a much narrower and smaller nasopharynx lumen compared to that of the adult. From Fig. 4a, the NP cross-sectional area of the infant (i.e., A = 78 mm^2) and child (i.e., A = 170 mm^2) is only one seventh and one third that of the adult (i.e., A = 535 mm^2) respectively. From Fig. 4c, the NP hydraulic diameter of the infant (i.e., 8.1 mm) and the child (i.e., d_h = 12.2 mm) is about one third and half that of the adult (i.e., d_h = 24.0 mm), respectively. Secondly, the distance to the nasal valve (the minimum cross-sectional area) is much shorter for the 9-month infant (11.2 mm, blue solid arrow in Fig. 4a) compared to the 5-year-old child (20.8 mm, black arrow) and adult (27.2 mm, red arrow). Similarly, the nasal valve area is also much smaller for the infant (i.e., ~56 mm^2) compared to both the child and adult, while the later two subjects have similar valve areas (i.e., ~180 mm^2) (Fig. 4a). This observation may imply that the nasal valve matures at early ages (around 5 years old). Another similar observation is for the nasal turbinate region, where the hydraulic diameter of the child and adult are very close (~10.0 mm) while that of the infant is much smaller (~3.8 mm).

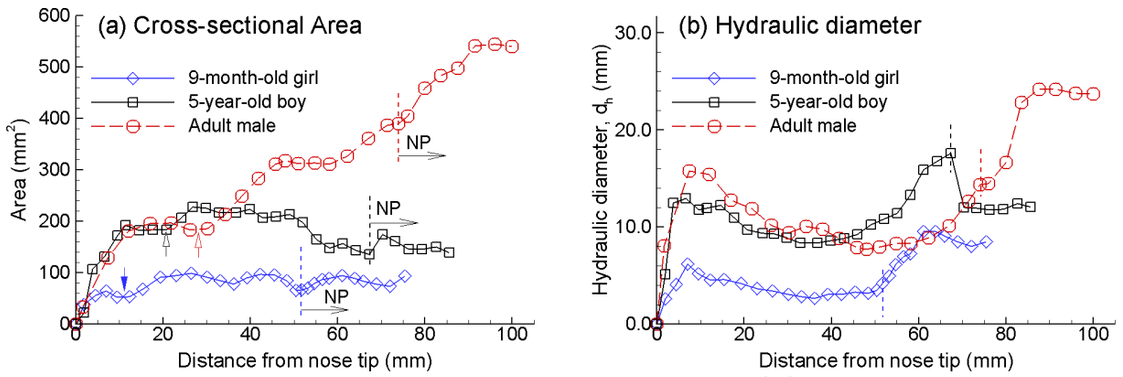

Fig. 4. Comparison of nasal cross-sectional area, perimeter, and hydraulic diameter between a 9-month-old girl, a five-year-old boy, and an adult male.

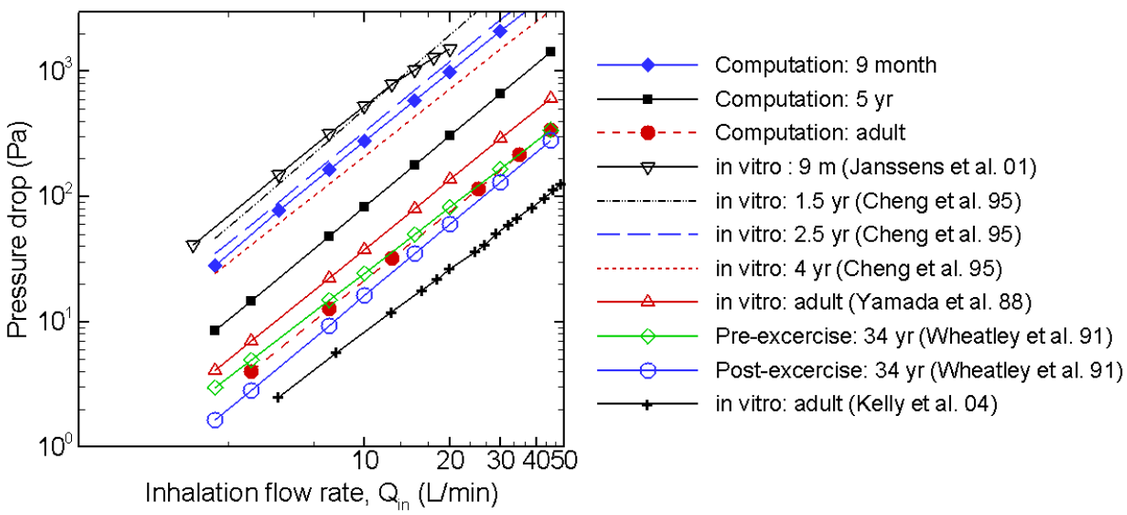

Fig. 5. Pressure drop (i.e., breathing impedance) as a function of inhalation flow rate with comparison to *in vitro* and *in vivo* measurements in various age groups.

3.2 Breathing resistance

Figure 5 shows the predicted breathing resistance (Δp) within the infant, child, and adult nasal airways considered in this study in comparison with existing *in vitro* and *in vivo* measurements for various age groups. *In vitro* data presented include an infant (9 month) (Janssens et al., 2001), young children (1.5 yr, 2.5 yr, 4 yr) (Cheng et al., 1995c), and adults (Kelly et al., 2004a; Yamada et al., 1988). *In vivo* data are from adult subjects (34 ± 5 yr) before and after exercise (Wheatley et al., 1991). In general, the pressure drop (i.e., breathing impedance) decreases as the age increases. Infants and children have much higher breathing impedance than adults for a same flow rate. As expected, the pressure drop curve of the 9-month infant agrees fairly well with the 9-month *in vitro* measurements (Janssens et al., 2001), and that of the 5-year-old boy falls between those of young children and adults. Children grow fast in height and weight before the age of seven and the rate of growth decreases thereafter, so does the growth of nasal airway. It is therefore reasonable that the infant breathing resistance is much higher while the 5-year-old breathing resistance is

somewhat between infants and adults. The pressure-flow relationships can be expressed as a power function ($\Delta P = a \cdot Q^b$), which can be plotted as straight lines on a log-log scale with slope "b". Table 4 lists the coefficients "a" and "b" for subjects of different ages. In light of the age-related effects, "a" constantly decreases in magnitude as age increases (from 8.87 at 9 month old to 0.54–0.16 when grown up) whereas the slopes of the Δp-Q_{in} curve are similar for all ages (b = 1.71–1.98).

Age/Reference	Method	a*	b*
9 m (Saint), Janssens (01)	*in vitro*, CT cast	8.87	1.75
9 m, This study	CFD, CT model	4.01	1.84
1.5 yr, Cheng (95)	*in vitro*, MRI cast	5.24±0.70	1.98±0.060
2.5 yr, Cheng (95)	*in vitro*, MRI cast	4.46±0.15	1.87±0.014
4 yr, Cheng (95)	*in vitro*, MRI cast	3.40±0.20	1.86±0.023
5 yr, This study	CFD, MRI model	1.07	1.89
Adult, Yamada (88)	*in vitro*, Cadaver cast	0.54	1.85
34 ± 5 yr, Wheatley (95)	*in vivo*, Pre-exercise	0.43±0.34	1.75±0.030
34 ± 5 yr, Wheatley (95)	*in vivo*, Post-exercise	0.20±0.35	1.90±0.028
53 yr, This study	CFD, MRI model	0.31	1.84
53 yr, Kelly (04)	*in vitro*, MRI cast, (nose only)	0.16	1.71

* $\Delta P\left(Pa\right) = aQ\left(L/\min\right)^b$

Table 4. Pressure drop (i.e., breathing impedance) in nasal airways at different ages,

3.3 Airflow field and particle transport

Comparison of airflow fields in the infant, child, and adult nasal airways are shown in Fig. 6 for an inhalation flow rate of 20 L/min. It is noted that this flow rate represents quite different physical activity conditions for the three subjects, i.e., light activity for the adult, medium activity for the child, and heavy activity for the infant. It is also noted that different velocity scale is used in each model. From Fig. 6, flows of high velocity magnitude are observed in the middle portion of the nasal passage for all the three models considered. In contrast, the narrow fin-like meatus regions receive a minimal fraction of the airflow, especially in the deeper portions of each meatus. The main flow changes its direction dramatically from the nostrils to the nasopharynx, forming a nearly 180^o curvature; however, this curvature is less severe for the infant model compared to the other two, preassembly resulting from a more back-tilted head position of the infant during image acquiring. No recirculation zone is observed in the infant and child NP due to a much smaller airway diameter in this region, which is different from the adult NP where flow recirculation is obvious (Xi and Longest 2008).

To compare secondary velocity motions of the three models considered, two-dimensional stream traces are plotted in the anterior and posterior passages of each model (Slices 2-2′ and 3-3′). Due to the thin air channels, vortices are damped and not discernable in the nasal passage. The magnitude of the secondary velocity in each slice is approximately 10% - 30% of the main flow. It is interesting to note that the relative strength of the second motion

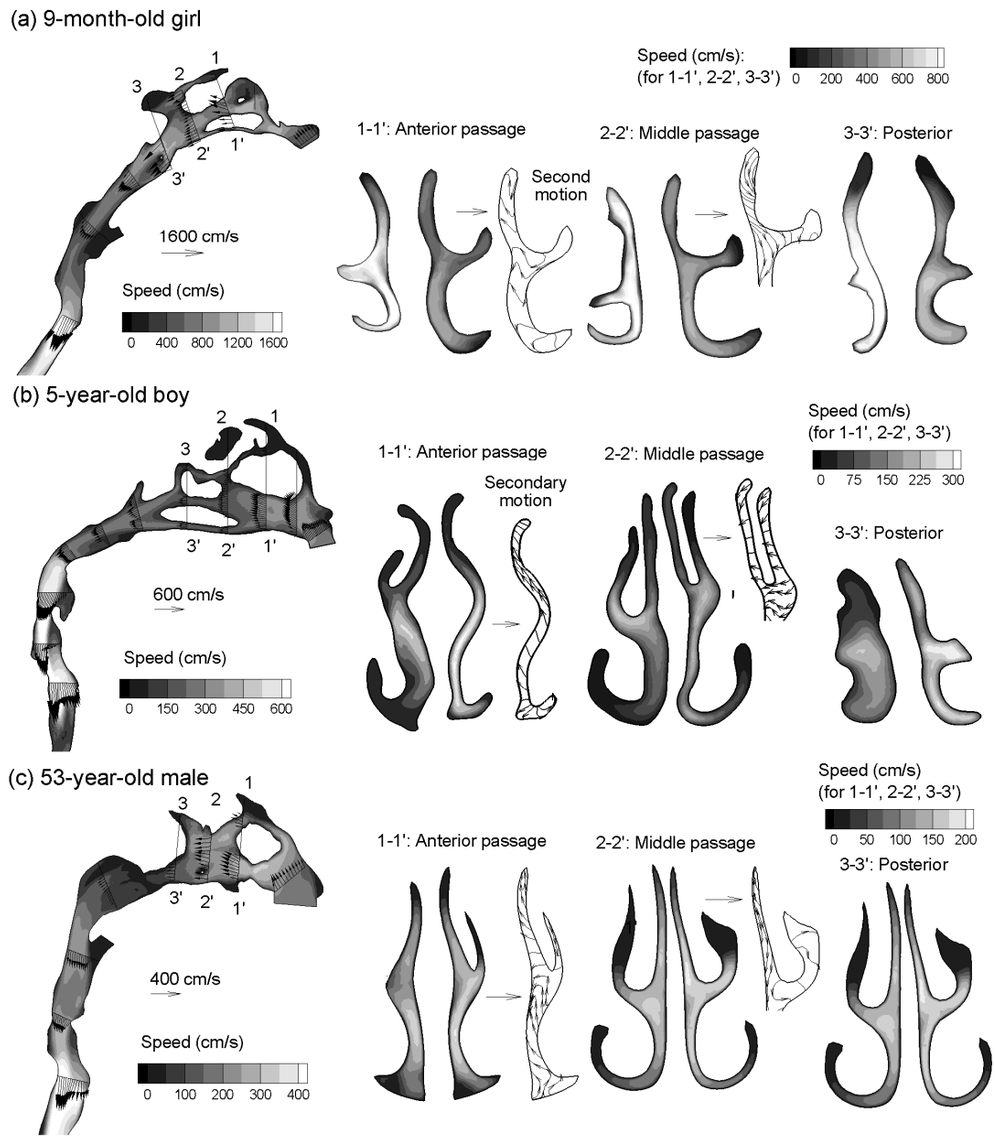

Fig. 6. Velocity fields in the nasal passages of the infant, child, and adult at 20L/min.

varies among the three age groups, which progressively increases as age increases. Take the middle passage (Slice 2-2′) as an example. The ratio of the secondary velocity to the mean speed is 3.6 to 25% with a median of 16% for the 9-month infant, 9.8 - 36% with a median of 25% for the 5-year-old child, and 13 to 40% with a median of 29% for the adult. The secondary motion functions to distribute the inhaled air into each fin-like meatus. Therefore, this difference might reflect the more matured (and more complicated) nasal turbinate at elder ages that more effectively convey the airflow throughout the nasal passages. Of particular interest is the observation of transportation of airflow toward the olfactory region. The secondary flows move upward prior to the olfactory region (Slice 2-2′) and downward after the olfactory region (Slice 3-3′). It is expected that the secondary motion near the olfactory region is delicately balanced, which should be large enough to convey a sufficient amount of particles or vapors for the olfactory nerve to perceive while still remaining small

enough to protect this extremely sensitive area that is directly connected to the brain. It is also interesting to note that the right and left nasal passages are quite different both in geometry and flow fields for all the three models considered, with one passage being more constricted than the other (Fig. 6). This geometric disparity is possibly attributed to the natural nasal cycle during which the airway obstruction alternates over a period of several hours (Eccles 1996). The resulting difference in airflows between the right and left passages has been suggested to help the central nerve system to locate where smell comes from.

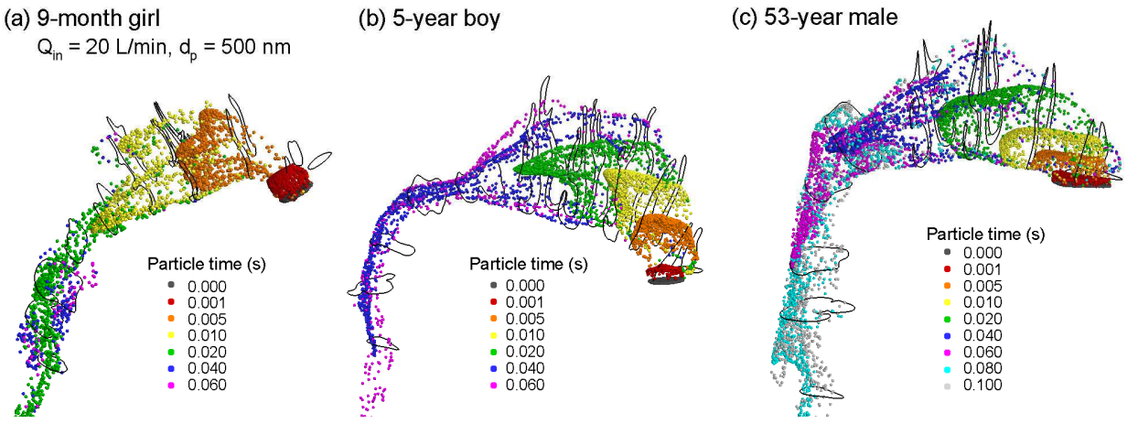

Fig. 7. Snapshots of particle locations through the right nasal passage of (a) 9-month-old girl, (b) 5-year-old boy, and (c) 53-year-old male. For each model, an amount of 2,000 particles of 500 nm were released at the right nostril at t = 0 ms and recorded at various instants.

Particle transport within the right nasal passage of the three models considered are visualized in Fig. 7 as snapshots of particle locations at specified instants for an inhalation flow rate of 20 L/min. Two thousand 500 nm particles were released at the right nostril at t = 0 ms and particle positions were recorded after designated period of times. Due to the small inertia and diffusion of the aerosols considered, particles are assumed to closely follow the airflow. For all the three models, faster transport and deeper penetration of aerosols are apparent in the medial passages while slow-moving particles are found near the airway walls. Because of the dramatic airway bend from the nostril to the nasopharynx, a high-concentration of particles constantly adjusts their directions following the mean streamline curvature of inhaled airflows. Considering that 20 L/min represents different levels of physical activity for the three subjects considered, the time required for the aerosols to fill the nasal airway also varies. It takes about 20 ms for particles to first reach the upper trachea for the infant (green symbols), whereas it takes 60 ms for the child, and 100 ms for the adult. The seemingly random particle distributions downstream of the nasopharynx indicate enhanced turbulent mixing in those regions. Due to the small-sized nasopharynx-larynx in both the infant and child, particles in this region are transported at a much higher rate than in adult (i.e., from NP to larynx taking 10 ms for the infant, 20 ms for the child, vs. 40 ms for the adult).

3.4 Particle deposition

Comparison of surface depositions in the infant, child, and adult nasal airways are shown in Fig. 8 for aerosols within both ultrafine (1–10 nm) and fine (100–1,000 nm) regimes at a constant inhalation flow rate of 20 L/min. Overall, much similarity than difference was

observed in the three models considered, whose deposition patterns exhibit much less heterogeneity than that we observed for micron particles (Xi et al., 2011). As expected, a large amount of ultrafine aerosols deposit in the nasal airways for all the models considered, while only a small amount of fine-regime aerosols deposit. In light of local depositions, ultrafine aerosols accumulate either in turbinate region or pharynx-larynx region, while the fine-regime aerosols accumulate mainly in the pharynx-larynx region where turbulence is most pronounced. One explanation for the ultrafine particle accumulation in the turbinate region is the narrow airway channel with the high particle diffusivity that disperses ultrafine particles onto the turbinate walls.

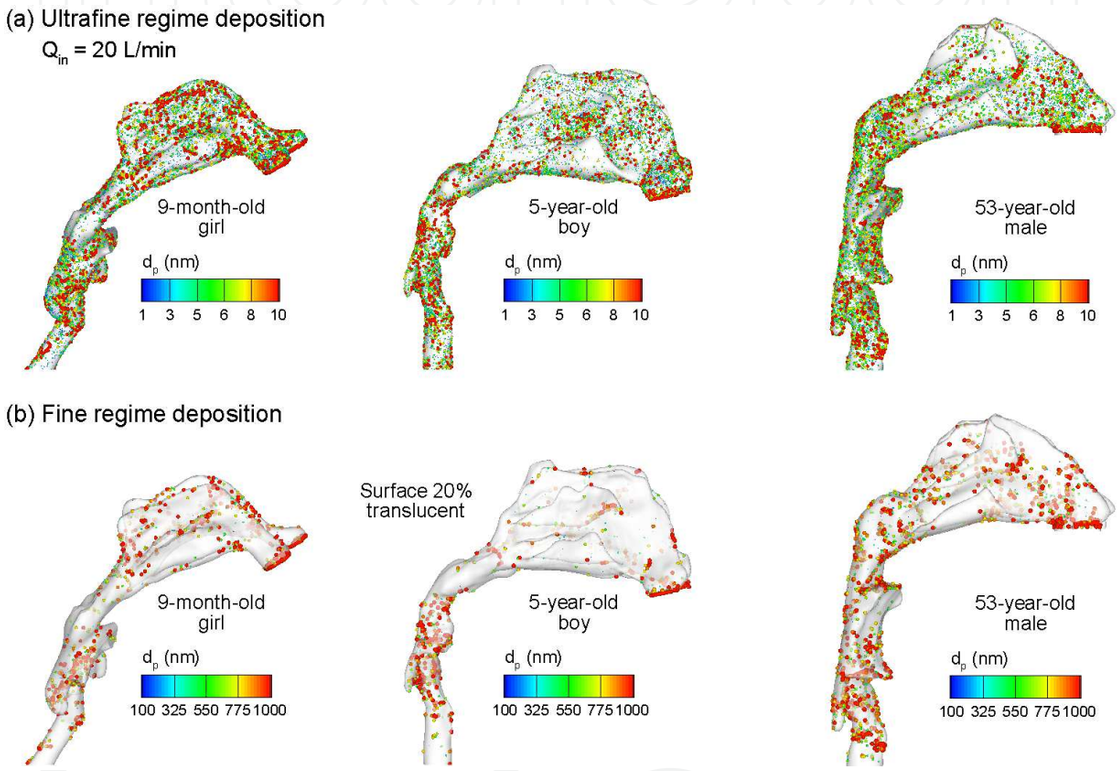

Fig. 8. Surface deposition in the three models of particles of (a) ultrafine regime (1 nm to 10 nm only) and (b) fine regime (100 nm to 1,000 nm). The fine-regime depositions are shown with 50% translucence.

Figure 9 shows the 3-D surface plot of the deposition fractions in the infant, child, and adult nasal airways as a function of both inhalation flow rate and particle size. The inhalation flow rates considered are 3, 5, 7.5, 10, 15, 20, 30, 45 L/min and the particle sizes are in the range of 1–1,000 nm. The three surface plots look alike both in trend and magnitude, with declining deposition rate as the particle size and flow speed increase. The peak deposition rate occurs at the smallest particle size and lowest flow rate considered (d_p = 1 nm and Q_{in} = 3 L/min) where the Brownian motion and residence time of the particles are both maximal. However, the relative role of the convective (flow rate) and molecular (particle size) diffusion differs in the ultrafine aerosol deposition, as the effect of molecular diffusion apparently overweighs that of convection for the breathing conditions considered herein. Considering the fine regime particles in the range of 100–1,000 nm, very low deposition fractions are observed for

all models considered. However, further examination of Fig. 9 reveals an interesting phenomenon associated with the interactions between mechanisms of diffusion and inertial impaction. For all three models considered, the deposition rate decreases first and then starts to increase with increasing particle size and flow rate. This valley-shaped profile results from a competition between the diminishing diffusive effect and enlarging finite inertial effect as the particle size and flow rate continuously rise, with the minimum occurring when the sum of these two effects is the smallest. But the breathing scenario of minimal deposition varies for the three age groups, which is at the inhalation flow rate of ~3 L/min for the infant and child, and is ~10 L/min for the adult, as shown in Fig. 9.

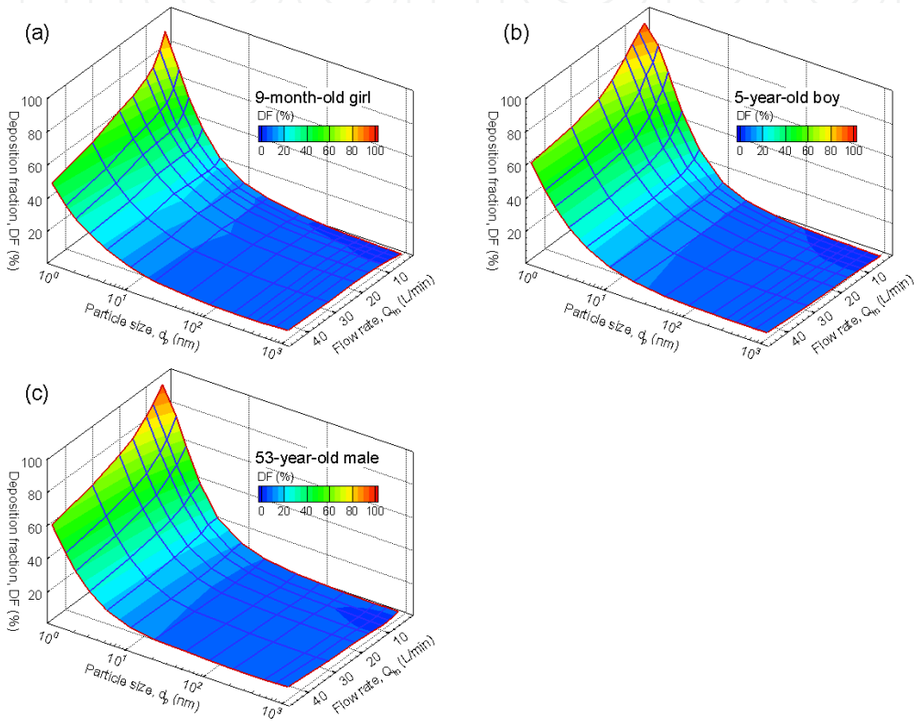

Fig. 9. 3-D surface plot of the total deposition fractions as a function of particle diameter and inhalation flow rate in the nasal-laryngeal airway models of (a) 9-month-old girl, (b) 5-year-old boy, and (c) 53-year-old male.

To further evaluate the predicted deposition results, the same data set from Fig. 9 has been plotted as a function of two existing diffusion parameters proposed from *in vitro* and *in vivo* deposition studies (Fig. 10). The first parameter ($D^{0.5}Q^{-0.125}$) was theoretically derived by Cheng et al. (1988) based on the assumption of turbulent diffusion in pipe flow and was later adopted in a series of *in vitro* replica studies (Cheng et al., 1995b; Cheng et al., 1993; Cheng et al., 1996b). The second parameter ($D^{0.5}Q^{-0.28}$) was later derived by Cheng et al. (2003) based on *in vivo* nasal deposition data, which exhibited a greater dependence on flow rate (i.e., exponent of -0.28) than the replica-based parameter (i.e., exponent of -0.125). Figures 10a and 10b shows the comparison of deposition profiles for the 53-year-old adult plotted as a function of the above two diffusion parameters. It is noted from Fig. 10a that the deposition results do not fully collapse for different flow rates and particle sizes, suggesting that the replica-based parameter ($D^{0.5}Q^{-0.125}$) does not accurately account for the relative

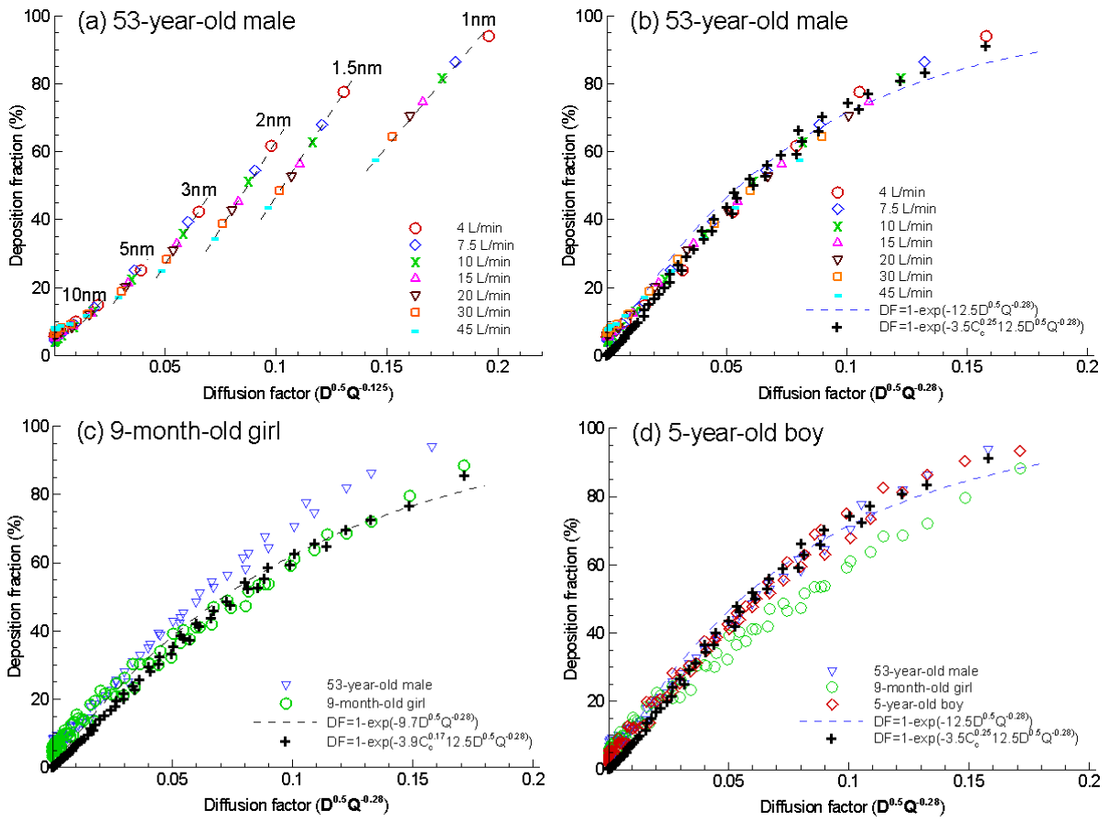

Fig. 10. Comparison of the deposition fractions as a function of the diffusion factor based on existing (a) *in vitro* ($D^{0.5}Q^{-0.125}$) and (b) *in vivo* ($D^{0.5}Q^{-0.28}$) studies in the male adult model. Inclusion of the Cunningham correction factor (C_c) improves agreement between the correlation and numerical data (b). The deposition fractions and associated correlations for (c) 9-month-old girl and (d) 5-year-old boy are also shown as a function of ($D^{0.5}Q^{-0.28}$). Units: Q [L/min] and D [cm²/s].

effect from convection and diffusion. In contrast, a more precise correlation was obtained by plotting the results as a function of the *in-vivo*-based parameter ($D^{0.5}Q^{-0.28}$). Following the format of the *in vivo* empirical correlation suggested by Cheng et al. (2003), $DF = 1 - exp(-a\, D^{0.5}Q^{-0.28})$, a coefficient of $a = 12.5$ was obtained for the 53-year-old deposition results (Fig. 10b). The resulting R^2 value was 0.92, indicating reasonably good agreement between the numerical data and the proposed empirical correlation. However, deviations becomes noticeable from $D^{0.5}Q^{-0.28} = 0.11$ and aggravates thereafter. Considering that deposition in the diffusion regime was also affected by non-continuum effects, the Cunningham correction factor C_c was incorporated into the diffusion parameter as ($C_c{}^b D^{0.5}Q^{-0.28}$) (Xi and Longest 2009). Again, an equation of $DF = 1 - exp(-c\, C_c{}^b D^{0.5}Q^{-0.28})$ was used to fit the expiratory simulation data. The best-fit values of b and c were 0.25 and 3.5, respectively, resulting in $R^2 = 0.98$ (Fig. 10b). The resulting ultrafine regime correlation in the nasal-laryngeal airways for adult is expressed as

$$\text{Adult: } DF = 1 - \exp(-3.5 C_c^{0.25} D^{0.5} Q^{-0.28}) \tag{3}$$

As evident from Fig. 10a and b, inclusion of the Cunningham correction factor results in a better approximation of the numerical data in comparison to the *in-vivo*-based correlation (Fig. 10b), and represents a significant improvement over the replica-based profile in Fig. 10a.

Figures 10c and 10d show the predicted deposition results as a function of $D^{0.5}Q^{-0.28}$ for the 9-month infant and 5-year-old child, respectively. The adult deposition data are also superimposed in these two plots to emphasize the age-related effects. Likewise, better approximations are obtained by including the Cunningham factor for the deposition results of the infant and child, which for the infant is expressed as

$$\text{9-month-old infant: } DF = 1 - \exp(-3.9C_c^{0.17}D^{0.5}Q^{-0.28}) \tag{4}$$

For a given value of diffusion factor ($D^{0.5}Q^{-0.28}$), the deposition results of the infant falls below those of the child and adult, while results of the child and adult appear to collapse into a single curve. As such, the correlation (Eq. 3) is also applied to the 5-year-old child model in this study.

3.5 Sub-regional and local depositions

Sub-regional deposition fractions within specific sections of the nasal airway are illustrated in Figs. 11-13. The sub-regions considered include nasal vestibule and valve (V&V), turbinate region (TR), nasopharynx (NP), pharynx, and larynx, as illustrated in Fig. 2. Figure 11 shows the surface plot of the sub-regional deposition fractions as a function of particle diameter and inhalation flow rate in the 9-month infant model. Surface plots in the child and adult models appear similar and are not shown. Unlike the total deposition plot in Fig. 9a, the flow-deposition response is noted to vary at each sub-region. In the nasopharynx (NP), the deposition fractions appear independent of the flow rate and being a function of particle diameter only (Fig. 11a). Furthermore, in the pharynx region, reduced ultrafine depositions are observed for smaller flow rates, which is opposite to the total deposition plot (Fig. 11 d vs. Fig. 9). This seemingly contrary observation is partially due to the fact that at low flow rates the majority of ultrafine particles entering the nose have deposit in the vestibule and turbinate regions already, leaving only a small amount of particles to deposit in the downstream regions. This depleting mechanism of particles into the anterior nasal passages is more pronounced at even lower inhalation flow rates.

Comparison of sub-regional deposition among the infant, child, and adult models is shown in Fig. 12 for varying particle sizes and in Fig. 13 for varying flow rates. For a same flow rate (15 L/min in Fig. 12), deposition rate consistently decreases with enlarging particles in each sub-region considered. However, this consistency is missing as to the flow rate effect upon the sub-regional deposition for an identical particle size (Fig. 13). Many factors could contribute to the erratic flow-deposition relations in Fig. 13 such as turbulence intensity, secondary motion, particle depletion in upstream regions, etc. In light of age effects, one observation is noteworthy: the deposition partition among the four sub-regions (i.e., turbinate, nasopharynx, pharynx, and larynx) is different for the three airway models. For example, in the turbinate region, the 5-year-old child model receives the highest deposition while the adult model receives the least for all particle sizes and flow rates considered (Figs. 12a, 13a). While in the larynx, the 5-year-old model receives less than the other two models.

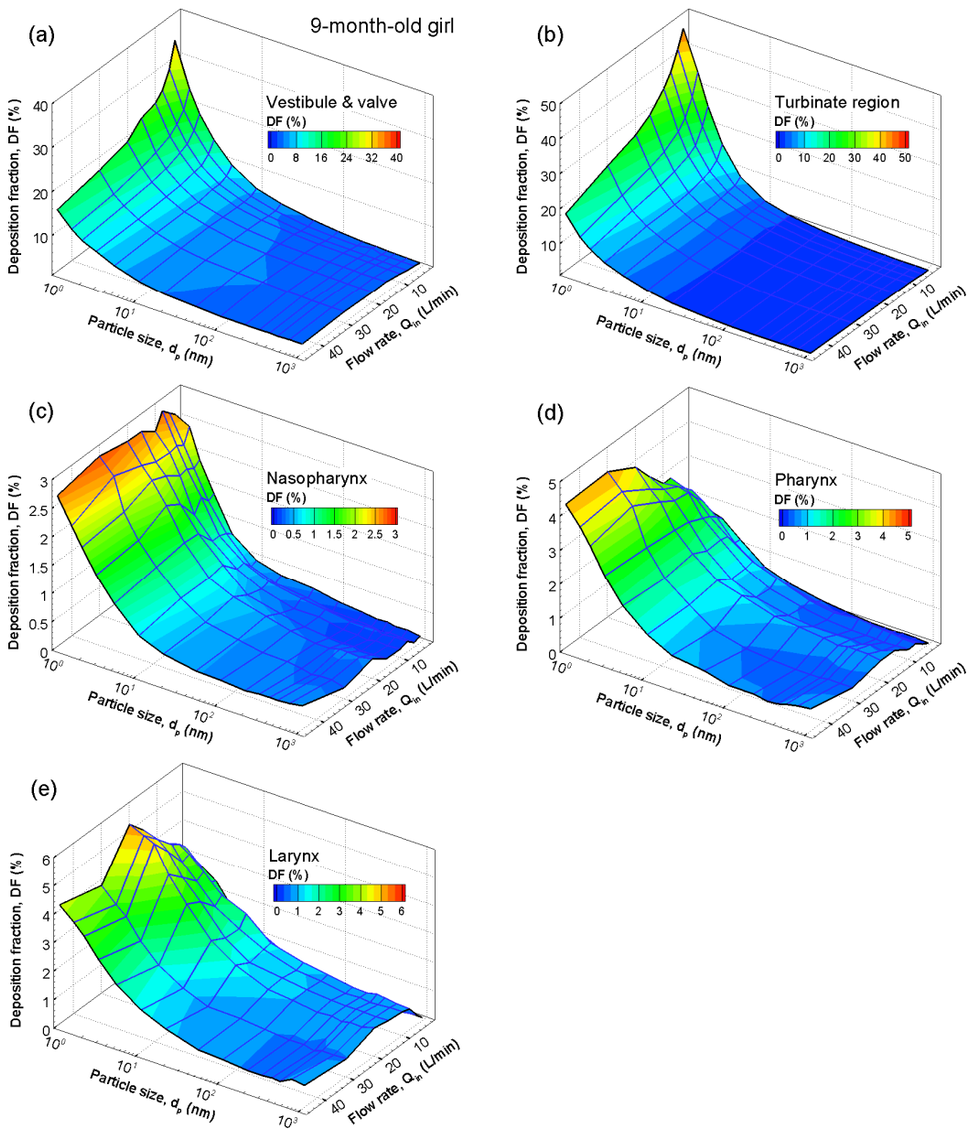

Fig. 11. 3-D surface plot of the sub-regional deposition fractions as a function of particle diameter and inhalation flow rate in the 9-month girl model at the site of (a) nasal vestibule and valve region, (b) turbinate region, (c) nasopharynx, (d) pharynx, and (e) larynx.

Mechanisms behind these irregular partitions could be complex. For example, the nasopharynx in adult has a much larger size and receives a twice larger deposition than in the infant and child. In contrast, the pharynx in child is smallest in size while receives the highest deposition among the three. This finding is worthy of our further attention. For inhalation toxicology, it means a different burden on the region of interest among different age groups. Meanwhile, for inhalation therapy that targets drugs at designated site of the respiratory system, this finding implies that existing adult deposition results might not guarantee an accurate dose planning for children and infants.

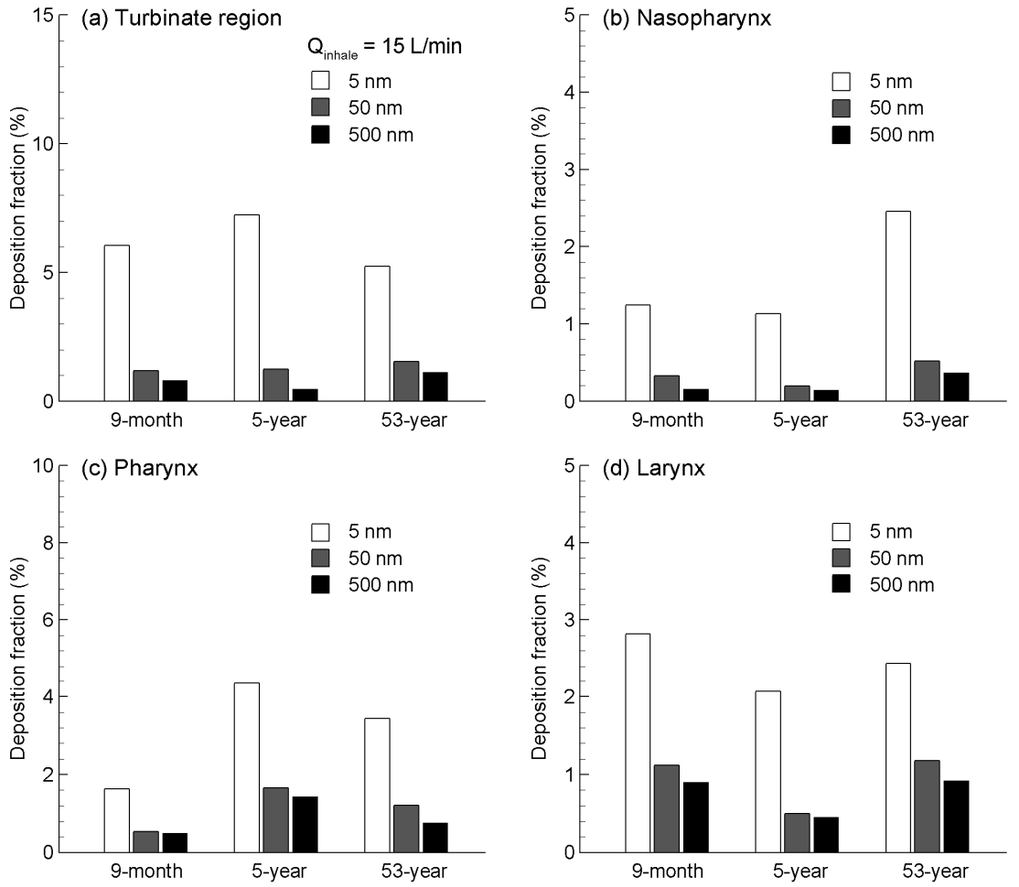

Fig. 12. Comparison of sub-regional deposition fractions between the three models (9-month, 5-year, 53-year) for different particle sizes (5 nm, 50 nm, and 500nm) at the site of (a) turbinate region, (b) nasopharynx, (c) pharynx, and (d) larynx.

To highlight the age-related effects on microdosimetry, a comparison of deposition enhancement factor (DEF) values among the infant, child, and adult models is illustrated in Fig. 14 for particles of 5 nm and an inhalation flow rate of 20 L/min. As discussed, the DEF value quantifies the particle dosage over an area of 50 airway epithelial cells in length with respect to the average deposition rate. The maximum DEF values are of the same order of magnitude for the three subjects considered, i.e. 26 – 41, with the youngest subject having the highest DEF value. This is in contrast with the highly concentrated accumulations of micron aerosols observed in the 5-year-old child model (Xi et al., 2011), which is one order of magnitude higher (i.e., DEF_{max} = 830 for 10 μm particles and 10 L/min flow rate). The overall pattern of deposition enhancement appears very similar for these three models. Each model exhibits hot spots on the dorsal walls of the larynx where convective diffusion is high due to converging airflow to the narrow glottis. Other hot spots with less elevated DEF values are observed for each model in the turbinate region. It is also noted that the nasal valve and pharyngeal dorsal wall do not have significant hot spots, which was the case for 10 μm aerosols (Xi et al., 2011). This lack of hot spots in the valve and pharynx regions is due to the negligible inertial impaction effect for ultrafine particles which can closely follow the main flow and easily maneuver through the constricted or highly curved passages.

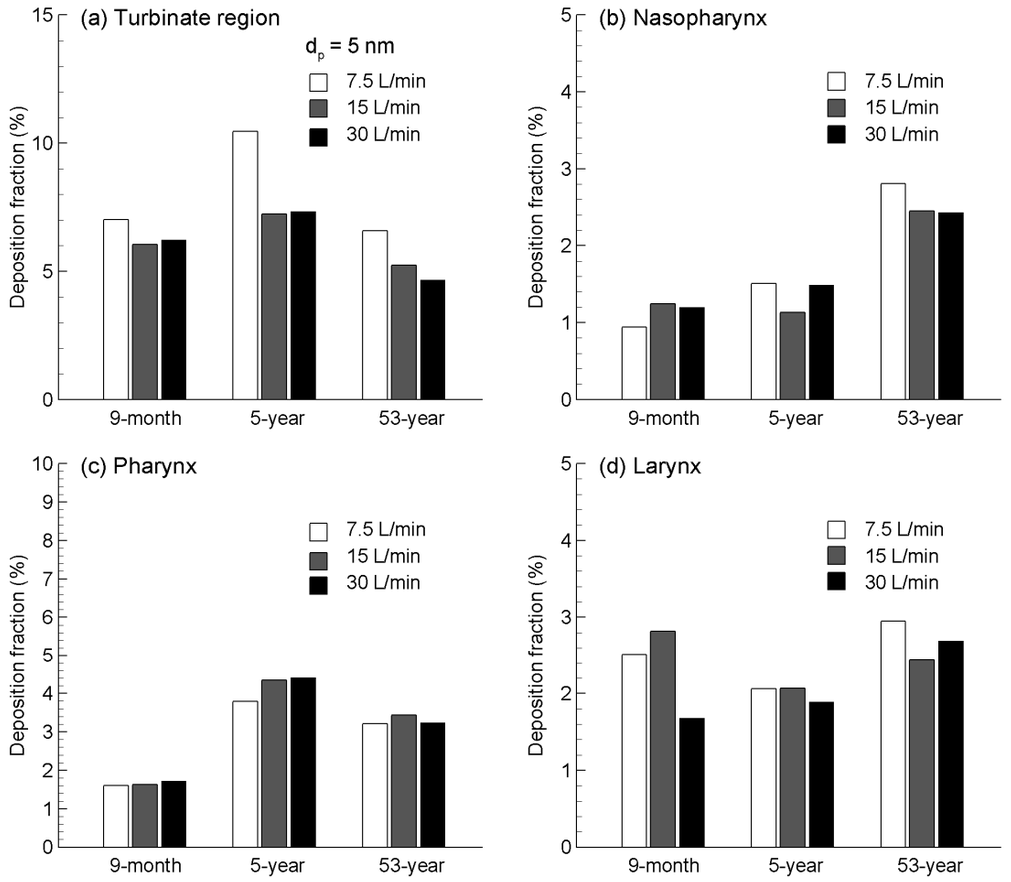

Fig. 13. Comparison of sub-regional deposition fractions between the three models (9-month, 5-year, 53-year) for different inhalation flow rates (7.5 L/min, 15 L/min, and 30 L/min) at the site of (a) turbinate region, (b) nasopharynx, (c) pharynx, and (d) larynx.

Local depositions for nanoparticles of sizes other than 5 nm and for different breathing conditions have been studied but not shown. Generally, it is found that for larger nanoparticles, existing hot spots shrink in size and become more concentrated due to rising particle inertia while deposition in other areas becomes more uniform due to decreased particle diffusivities. For 100 nm aerosols, hot spots reduce to regions only surrounding the glottis. Further, particles are more evenly distributed for heavier activity conditions.

4. Discussion

Significant differences were noted of the nasal anatomy among the infant, child, and adult subjects considered. These differences manifest themselves not only in airway dimension but also in airway morphology. For example, the nasal airway volume of the 9-month-old infant and the 5-year-old child is 18.8% and 40.3% that of the adult, respectively. At the same time, the infant and child have smaller sized nostrils, a shorter turbinate region, and a much slender nasopharynx. Results of this study indicate that the nasal valve and vestibule region might mature around the age of five. This is supported by the much shorter nostril-valve distance (i.e., 11.2 mm for infant *vs.* 20.8 mm for child and 27.2 mm for adult) and

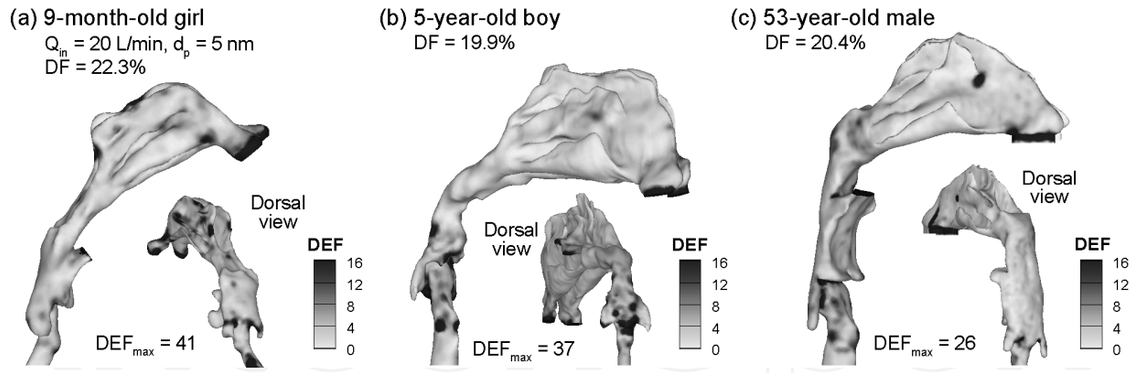

Fig. 14. Comparison of deposition enhancement factors (DEF) at Q_{in} = 20 L/min and d_p = 5 nm in (a) 9-month-old girl, (b) 5-year-old boy, and (c) 53-year-old male.

much smaller valve cross-sectional area (i.e., 56 mm^2 for infant vs. ~180 mm^2 for child and adult) of the 9-month infant compared to the 5-year-old child and adult (Fig. 4). The turbinate region experiences fast growth from birth to the age of five as indicated by the remarkable volume increase of this region in Table 2 (i.e., 2.83 cm^3 for infant, 11.03 cm^3 for child, and 12.63 cm^3 for adult); however, a lack of similarity in shape between the child and adult may still mean an undeveloped turbinate. It is apparent that the nasopharynx grows the least during the first five years (i.e., volume = 1.74 cm^3 for infant, 3.95 cm^3 for child, and 16.33 cm^3 for adult, Table 2). These child-adult discrepancies necessitate studies of specific age groups, or of the associated age effects.

Respiratory disorders are diverse in etiology and manifestations. Knowing detailed deposition information will greatly facilitate causality identification and dose-response assessment. The sub-regional and localized deposition values herein, which are amongst the first studies characterizing the detailed depositions in infants and children, have implications in narrowing down or pinpointing the site of highest possibility site (SHP) for respiratory lesions. These deposition hot spots are most susceptible to cancer formation, and are therefore extremely important to identify. For instance, a recent report by the National Research Council (NRC 2008) indicates that the *in vivo* response to inhaled bioaerosols is largely dependent on the site of local particle deposition within the respiratory tract. In this study, the deposition hot spots occur mainly on the turbinate and the dorsal wall of the larynx. Besides, the deposition partition in sub-regions (i.e., turbinate, nasopharynx, pharynx, and larynx) is quite different among the three age groups, indicating a different level of burdens upon the region of interest even when exposed to the same environment. From the drug delivery perspective, this difference finding implies that existing adult deposition results might not guarantee an accurate dose planning for children and infants.

While multiple empirical correlations of nasal nanoparticle depositions exist for adult and to a lesser extent for children, correlations including the age-related effects have rarely been reported. A significant issue in accounting for age effects is to determine the appropriate parameter that best represents the variations of nasal morphology and dimension with age. This parameter could be biological data such as age, height, weight, head circumference, or nasal airway data itself such as volume, surface area, hydraulic diameter, or even a combination of the two. Even though a single correlation applicable to all age groups is highly desirable, such a correlation has to be awaited until more nasal morphology and

deposition data become available for subjects of a large spectrum of ages. It is also a reminder (or caution) that there exist multiple ways in presenting/comparing/extrapolating deposition data in light of the age effects. For instance, besides the ventilation rate as in this study, deposition rates have also been compared in terms of physical activity level (Becquemin et al., 1991), per airway surface area (Diot et al., 1997), and per body mass (Phalen et al., 1991) depending on their comparison purpose. Considering the fact that terminologies defining the ventilation level are relatively arbitrary as no standard definitions exist (Phalen et al., 1985), comparing data from different studies is often not straightforward.

Limitations of this study include the assumptions of steady flow, simplified inlet conditions, ridge airway walls, and non-varying valve and glottal aperture. Other studies have highlighted the physical significance of transient breathing (Shi et al., 2006), inlet velocity profiles (Keyhani et al., 1995; Subramaniam et al., 1998), nasal wall motion (Fodil et al., 2005), nasal valve change (Bridger 1970; Bridger and Proctor 1970) and glottal aperture variation (Brancatisano et al., 1983; Xi et al., 2008). Moreover, each nasal model in this study is based on images of one single subject and does not account for the intersubject variability (Hilberg et al., 1993; Pickering and Beardsmore 1999). Another limitation is the typical supine position of the subjects during data acquisition, which is different from normal breathing while awake. Images are also taken at the end of the inhalation which may not reflect variations in airway geometry during a full breathing cycle. Therefore, future studies are needed that should be orientated toward: (1) improving physical realism and (2) including a broader population group. Our knowledge of nasal deposition is currently lacking in subpopulations such as pediatrics, geriatrics, and patients with respiratory diseases. Due to physiological development, aging, or diseases states, the airway anatomy can be remarkably different from that of a healthy adult. Concentrating on these specific subpopulations will help to clarify inter-group and inter-individual variability and will allow for the design of more efficient pharmaceutical formulations and drug delivery protocols. In particular, future *in vivo* and *in vitro* studies are needed to cross-validate numerical predictions before such results as in this study can be applied to clinical applications.

5. Conclusion

In conclusion, this study has assessed the age-related effects on airflows, breathing impedance, and submicrometer particle depositions in the nasal airways of a 9-month girl, a 5-year-old boy, and a 53-year-old male. A wide spectrum of breathing conditions (3–45 L/min) and aerosol sizes (1–1,000 nm) have been studied by means of numerical simulations. Specific findings of this study include:

1. Significant infant-child-adult discrepancies exist in the nasal airways in both morphology and dimension. Overall, the younger subject has smaller nostrils, a shorter turbinate region, and a slender nasopharynx. Besides, the 9-month infant has much shorter nostril-valve distance and much smaller valve cross-sectional area relative to the 5-year-old child and adult, while those of the later two subjects are similar in size, indicating a maturing of nasal valve at early ages (~ 5 years old). The nasal airway volume of the infant and child is 18.8% and 40.3% that of the adult, respectively; while the nasal airway surface area of the infant and child is 30.0% and 65.7% that of the adult, respectively.

2. Airflow in the main nasal passages was mostly laminar and transitional for all models considered at an inhalation flow rate of 20 L/min, with turbulence occurring mainly in the pharynx and larynx regions.
3. For a same flow rate, breathing resistance persistently decreases with rising age for the three models in this study. An empirical correlation for the breathing resistance was developed for different age groups based on a wide range of test conditions.
4. Insignificant variations in total and local depositions were found among the three models, even though discernible differences can still be noted for hot spot locations and intensities. However, the deposition partitioning in the sub-regions (i.e., turbinate, nasopharynx, pharynx, and larynx) was quite different among the three models considered.
5. Improved correlations of nasal deposition for ultrafine aerosols were developed for different age groups by implementing an *in vivo*-based diffusion parameter and the Cunningham correction factor. These correlations can also be applied to depositions of gases and vapors in the nasal airway for cases of rapid absorption on the airway surface.

6. References

Asgharian, B., Menache, M. G., and Miller, F. J. (2004) Modeling age-related particle deposition in humans. *Journal of Aerosol Medicine.* 17(3), 213-224.

Balashazy, I., Hofmann, W., and Heistracher, T. (1999) Computation of local enhancement factors for the quantification of particle deposition patterns in airway bifurcations. *Journal of Aerosol Science.* 30, 185-203.

Becquemin, M., Swift, D. L., Bouchikhi, A., Roy, M., and Teillac, A. (1991) Particle deposition and resistance in the noses of adults and children. *European Respiratory Journal.* 4(6), 694-702.

Bernstein, G. M. (2004) A review of the influence of particle size, puff volume, and inhalation pattern on the deposition of cigarette smoke particles in the respiratory tract. *Inhalation Toxicology.* 16, 675-689.

Brancatisano, T., Collett, P. W., and Engel, L. A. (1983) Respiratory movements of the vocal cords. *Journal of Applied Physiology.* 54(4), 1269-1276.

Bridger, G. P. (1970) Physiology of nasal valve. *Archives of Otolaryngology.* 92(6), 543-553.

Bridger, G. P., and Proctor, D. F. (1970) Maximum nasal inspiratory flow and nasal resistance. *Annals of Otology Rhinology and Laryngology.* 79(3), 481-488.

California EPA. (2005) *Proposed Identification of Environmental Tobacco Smoke as a Toxic Air Contaminant. Part B: Health Effects*, Sacramento, CA: California Environmental Protection Agency, Office of Environmental Health Hazard Assessment.

Cheng, Y. S., Yamada, Y., Yeh, H. C., and Swift, D. L. (1988) Diffusional deposition of ultrafine aerosols in a human nasal cast. *Journal of Aerosol Science.* 19, 741-751.

Cheng, Y. S., Su, Y. F., Yeh, H. C., and Swift, D. L. (1993) Deposition of Thoron progeny in human head airways. *Aerosol Science and Technology.* 18, 359-375.

Cheng, K.-H., Cheng, Y.-S., Yeh, H.-C., and Swift, D. L. (1995a) Deposition of ultrafine aerosols in the head airways during natural breathing and during simulated breath holding using replicate human upper airway casts. *Aerosol Science and Technology.* 23(3), 465-474.

Cheng, Y. S., Smith, S. M., Yeh, H. C., Kim, D. B., Cheng, K. H., and Swift, D. L. (1995b) Deposition of ultrafine aerosols and thoron progeny in replicas of nasal airways of young children. *Aerosol Science and Technology.* 23, 541-552.

Cheng, K. H., Cheng, Y. S., Yeh, H. C., Guilmette, R. A., Simpson, S. Q., Yang, S. Q., and Swift, D. L. (1996a) *In vivo* measurements of nasal airway dimensions and ultrafine aerosol depositing in human nasal and oral airways. *Journal of Aerosol Science.* 27, 785-801.

Cheng, Y. S., Yeh, H. C., Guilmette, R. A., Simpson, S. Q., Cheng, K. H., and Swift, D. L. (1996b) Nasal deposition of ultrafine particles in human volunteers and its relationship to airway geometry. *Aerosol Science and Technology.* 25(3), 274-291.

Cheng, Y. S. (2003) Aerosol deposition in the extrathoracic region. *Aerosol Science and Technology.* 37, 659-671.

Cohen Hubal, E. A., Kimbell, J. S., and Fedkiw, P. S. (1996) Incorporation of nasal-lining mass-transfer resistance into a CFD model for prediction of ozone dosimetry in the upper respiratory tract. *Inhalation Toxicology.* 8(9), 831-857.

Crawford, D. J. (1982) Identifying critical human subpopulations by age groups: radioactivity and the lung. *Physics in Medicine and Biology.* 27(4), 539-552.

Diot, P., Palmer, Lucy B., Smaldone, A., Decelie-Germana, J., Grimson, R., and Smaldone, Gerald C. (1997) RhDNase I aerosol deposition and related factors in cystic fibrosis. *American Journal of Respiratory and Critical Care Medicine.* 156(5), 1662-1668.

Eccles, R. (1996) A role for the nasal cycle in respiratory defence. *European Respiratory Journal.* 9(2), 371-376.

Everard, M. L. (2003) Inhalation therapy for infants. *Advanced Drug Delivery Reviews.* 55(7), 869-878.

Fodil, R., Brugel-Ribere, L., Croce, C., Sbirlea-Apiou, G., Larger, C., Papon, J. F., Delclaux, C., Coste, A., Isabey, D., and Louis, B. (2005) Inspiratory flow in the nose: a model coupling flow and vasoerectile tissue distensibility. *Journal of Applied Physiology.* 98(1), 288-295.

Gradon, L., and Yu, C. P. (1989) Diffusional particle depositoin in the human nose and mouth. *Aerosol Science and Technology.* 11, 213-220.

Guilmette, R. A., Cheng, Y. S., Yeh, H. C., and Swift, D. L. (1994) Deposition of 0.005 - 12 micrometer monodisperse particles in a computer-milled, MRI-based nasal airway replica. *Inhalation Toxicology.* 6 (Suppl. 1), 395-399.

Gurr J. R., Wang A. S. S., Chen C. H., Jan K.Y. (2005) Ultrafine titanium dioxide particles in the absence of photoactivation can induce oxidative damage to human bronchial epithelial cells. *Toxicology*, 213, 66-73.

Hilberg, O., Jensen, F. T., and Pedersen, O. F. (1993) Nasal airway geometry: comparison between acoustic reflections and magnetic resonance scanning. *Journal of Applied Physiology.* 75(6), 2811-2819.

ICRP. (1994) *Human Respiratory Tract Model for Radiological Protection*, Elsevier Science Ltd., New York.

Janssens, H. M., de Jongste, J. C., Fokkens, W. J., Robben, S. G., Wouters, K., and Tiddens, H. A. (2001) The Sophia Anatomical Infant Nose-Throat (Saint) model: a valuable tool to study aerosol deposition in infants. *Journal of Aerosol Medicine : The Official Journal of the International Society for Aerosols in Medicine.* 14(4), 433-41.

Keith, C. H. (1982) Particle size studies on tobacco smoke. *Beiträge zur Tabakforschung International/Contributions to Tobacco Research.* 11(3), 123-131.

Kelly, J. T., Asgharian, B., Kimbell, J. S., and Wong, B. (2004a) Particle deposition in human nasal airway replicas manufactured by different methods. Part I: inertial regime particles. *Aerosol Science and Technology.* 38, 1063-1071.

Kelly, J. T., Asgharian, B., Kimbell, J. S., and Wong, B. (2004b) Particle deposition in human nasal airway replicas manufactured by different methods. Part II: ultrafine particles. *Aerosol Science and Technology.* 38, 1072-1079.

Keyhani, K., Scherer, P. W., and Mozell, M. M. (1995) Numerical simulation of airflow in the human nasal cavity. *Journal of Biomechanical Engineering-Transactions of the Asme.* 117(4), 429-441.

Kittelson, D. B. (1998) Engines and nanoparticles: a review. *Journal of Aerosol Science.* 29(5-6), 575-588.

Kreyling, W. G., Semmler-Behnke, M., and Moller, W. (2006) Ultrafine particle-lung interactions: does size matter? *Journal of Aerosol Medicine.* 19, 74-83.

Kreyling, W. G., Semmler, M., and Moller, W. (2004) Dosimetry and toxicology of ultrafine particles. *Journal of Aerosol Medicine.* 17(2), 140-152.

Li, N., Sioutas, C., Cho, A., Schmitz, D., Misra, C., Sempf, J., Wang, M. Y., Oberley, T., Froines, J., and Nel, A. (2003) Ultrafine particulate pollutants induce oxidative stress and mitochondrial damage. *Environmental Health Perspectives.* 111(4), 455-460.

Liu, Y., Matida, E. A., Gu, J., and Johnson, M. R. (2007) Numerical simulation of aerosol deposition in a 3-D human nasal cavity using RANS, RANS/EIM, and LES. *Journal of Aerosol Science.* 38, 683-700.

Longest, P. W., and Xi, J. (2007) Effectiveness of direct Lagrangian tracking models for simulating nanoparticle deposition in the upper airways. *Aerosol Science and Technology.* 41, 380-397.

Lumb, A. B. (2000) *Nunn's Applied Respiratory Physiology*, Butterworth Heinemann, Oxford.

Mandell, G. L., Bennett, J. E., and Bolin, R. D. (2004) *Principles and Practices of Infectious Diseases*, Churchhill Livingstone, New York.

Martonen, T. B. (1986) Surrogate experimental models for studying particle deposition in the human respiratory tract: an overview. *Aerosols*, S. D. Lee, ed., Lewis Publishers, Chesea, Michigan.

Martonen, T. B., Zhang, Z. Q., Yue, G., and Musante, C. J. (2003) Fine particle deposition within human nasal airways. *Inhalation Toxicology.* 15(4), 283-303.

Matida, E. A., Finlay, W. H., Lang, C. F., and Grgic, L. B. (2004) Improved numerical simulation of aerosol deposition in an idealized mouth-throat. *Journal of Aerosol Science.* 35, 1-19.

Morsi, S. A., and Alexander, A. J. (1972) An investigation of particle trajectories in two-phase flow systems. *Journal of Fluid Mechanics.* 55(2), 193-208.

NRC. (2008) *A Framework for Assessing teh Health Hazad Posed by Bioaerosols*, The national Academies Press, Washington DC.

Oberdorster, G., and Utell, M. J. (2002) Ultrafine particles in the urban air: to the respiratory tract and beyond. *Environmental Health Perspectives.* 110(8), A440-A441.

Oldham, M. J., Mannix, R. C., and Phalen, R. F. (1997) Deposition of monodisperse particles in hollow models representing adult and child-size tracheobroncial airways. *Health Physics.* 72(6), 827-833.

Ostiguy, C., Soucy, B., Lapointe G., Woods. C., Menard, L., and Trottier M., (2008) Health effects of nanoparticles, seond edition, in *Chemical Substance and Biological Agents*, Report R-589, IRSST, Montreal.

Phalen, R. F., Cuddihy, R. G., Fisher, R. G., Moss, O. R., Schlesinger, R. B., Swift, D. L., and Yeh, H. C. (1991) Main features of the proposed NCRP respiratory tract dosimetry model. *Radiation Protection Dosimetry.* 38, 179-184.

Phalen, R. F., Oldham, M. J., Beaucage, C. B., Crocker, T. T., and Mortensen, J. D. (1985) Postnatal enlargement of human tracheobronchial airways and implications for particle deposition. *The Anatomical Record.* 212, 368-380.

Pickering, D. N., and Beardsmore, C. S. (1999) Nasal flow limitation in children. *Pediatric Pulmonology.* 27(1), 32-36.

Pritchard, S. E., and McRobbie, D. W. (2004) Studies of the human oropharyngeal airspaces using magnetic resonance imaging. II. The use of three-dimensional gated MRI to determine the influence of mouthpiece diameter and resistance of inhalation devices on the oropharyngeal airspace geometry. *Journal of Aerosol Medicine.* 17(4), 310-324.

Sayes, C. M., Gobin, A. M., Ausman, K. D., Mendez. J., West, J. L., Colvin, V. L. (2005) Nano-C60 cytotoxicity is due to lipid peroxidation. *Biomaterials*, 25, 7587-7595.

Scherer, P. W., Keyhani, K., and Mozell, M. M. (1994) Nasal dosimetry modeling for humans. *Inhalation Toxicology.* 6, 85-97.

Schroeter, J. D., Musante, C. J., Hwang, D. M., Burton, R., Guilmette, R., and Martonen, T. B. (2001) Hygroscopic growth and deposition of inhaled secondary cigarette smoke in human nasal pathways. *Aerosol Science and Technology.* 34(1), 137-143.

Shi, H., Kleinstreuer, C., and Zhang, Z. (2006) Laminar airflow and nanoparticle or vapor deposition in a human nasal cavity model. *Journal of Biomechanical Engineering.* 128, 697-706.

Subramaniam, R. P., Richardson, R. B., Morgan, K. T., Kimbell, J. S., and Guilmette, R. A. (1998) Computational fluid dynamics simulations of inspiratory airflow in the human nose and nasopharynx. *Inhalation Toxicology.* 10(2), 91-120.

Swift, D. L., and Strong, J. C. (1996) Nasal deposition of ultrafine 218Po aerosols in human subjects. *Journal of Aerosol Science.* 27(7), 1125-1132.

U.S. Surgeon General Report. (2007) *Children and Secondhand Smoke Exposure-Excerpts from The Health Consequences of Involuntary Exposure to Tobacco Smoke: A Report of the Surgeon General*, U.S. Department of Health and Human Services.

Wheatley, J. R., Amis, T. C., and Engel, L. A. (1991) Nasal and oral airway pressure-flow relationships. *Journal of Applied Physiology.* 71(6), 2317-2324.

Wilcox, D. C. (1998) *Turbulence Modeling for CFD, 2nd Ed.*, DCW Industries, Inc., California.

Xi, J., and Longest, P. W. (2007) Transport and deposition of micro-aerosols in realistic and simplified models of the oral airway. *Annals of Biomedical Engineering.* 35(4), 560-581.

Xi, J., and Longest, P. W. (2008) Numerical predictions of submicrometer aerosol deposition in the nasal cavity using a novel drift flux approach. *International Journal of Heat and Mass Transfer.* 51(23-24), 5562-5577.

Xi, J., Longest, P. W., and Martonen, T. B. (2008) Effects of the laryngeal jet on nano- and microparticle transport and deposition in an approximate model of the upper tracheobronchial airways. *Journal of Applied Physiology.* 104(6), 1761-1777.

Xi, J., and Longest, P. W. (2009) Characterization of submicrometer aerosol deposition in extrathoracic airways during nasal exhalation. *Aerosol Science and Technology.* 43(8), 808-827.

Xi, J., Longest, P. W., and Anderson P. J. (2010) Respiratory aerosol dyanmics with applications to pharmaceutical drug delivery, in *Colloids in Drug Delivery,* Monzer Fanun (ed.), CRC Press Taylor & Francis, 501-526.

Xi, J., Si, X., Kim, J. W., and Berlinski, A. (2011) Simulation of airflow and aerosol deposition in the nasal cavity of a 5-year-old child. *Journal of Aerosol Science.* 42(3), 156-173.

Xu, G. B., and Yu, C. P. (1986) Effects of Age on Deposition of Inhaled Aerosols in the Human Lung. *Aerosol Science and Technology.* 5(3), 349-357.

Yamada, Y., Cheng, Y. S., Yeh, H. C., and Swift, D. L. (1988) Inspiratory and expiratory deposition of ultrafine particles in a human nasal cast. *Inhalation Toxicology.* 1, 1-11.

Yang, C. P., Callagher, R. P., Weiss, N. S., B and, P. R., Thomas, D. B., and Russel, D. A. (1989) Differences in incidence rates of cancers of the respiratory tract by anatomic subside and histological type: an etiologic implication. *Journal of National Cancer Institute.* 81(21), 1828-1831.

Yu, G., Zhang, Z., and Lessmann, R. (1998) Fluid flow and particle diffusion in the human upper respiratory system. *Aerosol Science and Technology.* 28, 146.

Zamankhan, P., Ahmadi, G., Wang, Z., Hopke, P. K., Cheng, Y. S., Su, W. C., and Leonard, D. (2006) Airflow and deposition of nano-particles in a human nasal cavity. *Aerosol Science and Technology.* 40, 463-476.

Zhao, K., Scherer, P. W., Hajiloo, S. A., and Dalton, P. (2004) Effects of anatomy on human nasal air flow and odorant transport patterns: implications for olfaction. *Chemical Senses.* 29(5), 365-379.

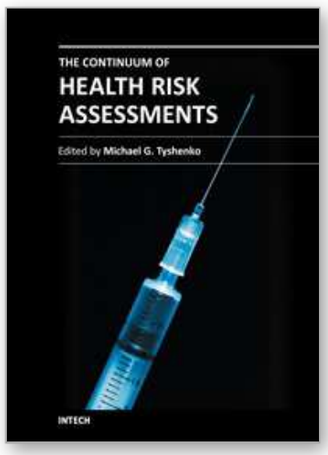

The Continuum of Health Risk Assessments
Edited by Dr. Michael G. Tyshenko

ISBN 980-953-307-582-7
Hard cover, 194 pages
Publisher InTech
Published online 16, May, 2012
Published in print edition May, 2012

This book presents a collection of health risk assessments for known and emerging hazards that span a continuum. Case studies for existing health risks include psychoactive drug usage in delivery truck drivers and using look-back risk assessment for accidental syringe re-use in healthcare settings. Case studies for emerging risks include precautionary actions to safeguard blood supplies; nanoparticle deposition in the lung; and the epistemic issues surrounding genetically modified organism risk assessments. The final section of the book deals with advancing health risk assessment analyses through a post-genomics lens and provides case studies on personalized genomics, new data analyses and improving in silico models for risk assessment. These case studies provide much insight into the ongoing evolution of health risk assessments.

INTECH
open science | open minds

InTech Europe
University Campus STeP Ri
Slavka Krautzeka 83/A
51000 Rijeka, Croatia
Phone: +385 (51) 770 447
Fax: +385 (51) 686 166
www.intechopen.com

InTech China
Unit 405, Office Block, Hotel Equatorial Shanghai
No.65, Yan An Road (West), Shanghai, 200040, China
中国上海市延安西路65号上海国际贵都大饭店办公楼405单元
Phone: +86-21-62489820
Fax: +86-21-62489821

IntechOpen